Deformational characteristics of a high-vacuum insulation panel

Hung-Shan Shu† and Yang-Cheng Wang‡

*Department of Civil Engineering, Chinese Military Academy, 1 Hwang-Poo Road,
Feng-Shan, 83000, Taiwan, R.O.C.*

Abstract. The objective of this study is to analyze the deformational characteristics of a high-vacuum insulation panel that is evacuated to eliminate significant gas-phase conductance through its thickness. The panel is composed of a metal envelope and low thermal conductance spacers. The problem is very challenging because several nonlinearities are involved concurrently. Not only are various finite element models such as triangular, rectangular, beam and circular plate models used to simulate the panel, but also several finite element programs are used to solve the problem based on the characteristics of the finite element model. The numerical results indicate that the effect of the diameter of the spacer on the vertical deformation of the plate panel is negligibly small. The parameter that mainly influences the maximum sag is the spacing between the spacers. The maximum vertical deformation of the panel can be predicted for a practical range of the spacing between the spacers and the thickness of the plate. Compared with the numerical results obtained by the finite element models and the experimental tests, they have a good agreement. The results are represented in both tabular and graphical forms. In order to make the results useful, a curve fitting technique has been applied to predict the maximum deformation of the panel with various parameters. Moreover, the panel was suggested to be a "smart" structure based on thermal effect.

Key words: characteristics; vacuum; insulation; panel.

1. Introduction

A thin section, high-vacuum insulation panel, which consists of a thin plate panel that is evacuated to eliminate significant gas-phase conductance through its thickness, can be used in refrigerator-freezers, thermal bottle, and other applications. The panel is composed of a metal envelope and low thermal conductance spacers that are sparsely distributed between the metal sheets to maintain the desired distance between the sheets. Because spacers separate the metal sheets, the structural panel can be either flat or shaped to the geometry needed for the application. Heat transfer occurs by radiation, conductance through the spacers and conductance through the edges of the panel where the envelope is sealed. The structural requirements for the plate panel are:

1. To prevent physical contact between the plates that form the envelope;

2. To minimize the overall contact area of the spacers with the plates per unit surface area of the panel, either by decreasing the contact area between spacer and plates or by decreasing the overall number of the spacers;

---

† Lecturer
‡ Professor

3. To minimize the overall weight of the whole panel.

Nonlinear analysis usually can be categorized as four primary groups: geometric, materials, boundary, and force nonlinearities. In this paper, the problem is very challenging since this type of panel consists of several structural nonlinearities simultaneously such as the deformations, contact area between the plates and spacers. The analytical procedure is not convenient to solve this type of problem at present but numerical methods are feasible. Bathe (1982) indicates that during the past two decades, the finite element method of analysis has rapidly become a very popular technique for the computer solution of complex problem in engineering. At present, the finite element method represents a most general analysis tool and is used in practically all fields of engineering analysis. Therefore, four different finite element models such as triangular (Wei *et al*. 1995), rectangular, beam (Shu *et al*. 1997), and circular plate models are established to estimate the deformational characteristics: contact surface between the isolating sphere and the thin plate panel; the vertical deformation of the plates between the spheres.

To increase the rigidity of the plates and decrease the deformation of the panel, a new geometry is proposed. The deformation of the new geometry was analyzed with various geometric parameters. The sophisticated evaluation of the finite element modeling was performed to address the issues of boundary conditions, element size, element spacing, element type (Hua *et al*. 1997), and analysis type, etc.

Based on the deformational characteristics of the panel, various finite element programs and finite element models are used to analyze the panel. In this research effort, the following tasks were performed:

1. The vertical deformation between the consequent spacers is found to prevent the physical contact of the envelope plates.
2. The contact area between the panels and the spacers is estimated to minimize the overall contact area with various geometric parameters. It reduces the heat transfer through the contact areas.
3. The elastic-plastic material properties were applied to perform the stress distribution in order not to excess the allowable stress of the materials.
4. Once the tasks are achieved, the optimum supported pattern of the design panel is found based on the vertical deformations, stress distribution, and the minimum overall contact area.
5. Finally, the panel was suggested to be a "smart" structure based on thermal effect.

2. Problem statements

Because the plate panel consists of thin plates and spacers subjected to atmospheric pressure, the vertical deformation between consequent spacers, the contact areas between the plates and the spacers as well as the stress distribution of the elastic-plastic material are the most important tasks of this type of panel. In order to predict the structural behavior, four primary structural characteristics are investigated such as vertical deformation, overall contact area, stress distribution, and the optimum end support pattern.

2.1. Vertical deformation

The most important requirement of the structures is to prevent the physical contact between the plates. The first task of this paper is to estimate the vertical deformation of the panel under

atmospheric pressure between consequent spacers for various support-spacing S and the plate thickness t. Based on finite element methods, the maximum sag of the panels subjected to equivalent atmosphere pressure is found and curve fitting techniques have been employed to derive second or higher order formulas to predict the maximum sag for a given pair of S and t to make the results useful.

2.2. Contact area

The second most important requirement of the structural panel is to minimize the overall contact area of the spacers of the panel to reduce the heat conductance. It is important to be able to predict the contact area between the plate and the spacers under atmospheric pressure for various spacing S, the radius of the spacer R_c, and the thickness of the panel t. The structural characteristics of the local plasticity of the plate at the support points, the large deformations compared to the thickness, and a significant contact between two deformable bodies are taken into account. The contact radius R_c of the panel with the spacer is found. The results are also employed to derive fifth order formulas to predict the contact radius R_c for a range of practical values of S, R_c, and t.

2.3. Rigidity of the panel

In general, flat plates are not a desirable configuration to resist bending. An effort was made to examine potential rigidity schemes in order to minimize the maximum deformation of the structural panels. Due to the material nonlinearity, the stress distribution has been found. The vertical deformation and the stress distribution are always interacted. Therefore, the maximum deformation is one of the most important factors for the stress distribution.

2.4. Optimum supported patterns

The overall contact area between the plates and the spacers is another important requirement of this panel to prevent the heat conductance. The optimum supported pattern does not only reduce the overall contact area but also reduces the stress distribution and the vertical deformation of the plates.

2.5. Smart structure

Based on the idealization of no thermal expansion effects, the thermal effect of the deformation of the panel is ignored but the thermal effect of realistic structure must be taken into account in the further design if the structure serves as an isolator for high temperature variation. The temperature variation may create the interaction of these nonlinearities. Therefore, the design pattern of a smart structure is proposed based on the thermal effect of the deformational characteristics of this type of structures.

3. Finite element models

How to properly discretize the structure and how to properly simulate the boundary conditions are the most important factors of the finite element modeling. It is hardly to simulate a structure if it

involves several structural nonlinearities, simultaneously. Hua (1997) *et al.* illustrated the effects on structural modeling using different finite element models and different element types. Bathe (1982) indicated that it is the aim to establish the finite element procedures using relatively simple and physical concepts, even at the expense of losing some mathematical rigorousness. The problem described in this paper involves several types of nonlinearity such as material, geometric and boundary nonlinearities. In this paper, four finite element models are established using different element patterns and element types to specify the characteristics of the structure.

3.1. Problem idealization

In order accurately to make the analysis, the idealizations of the structure are made as follows:

1. The panel is originally flat and the spacer is a perfect sphere. The penetration of the sphere is not allowed.

2. The panel material is isotropic. If it is linearly elastic, the modulus of elasticity is taken either E=195000 or 200000 N/mm^2 and Poisson's ratio v=0.3. If it is elastic-plastic, the tangent modulus E_t=1.0 kN/mm^2, the yield stress σ_y=276 N/mm^2. The spacer material is isotropic, linearly elastic with the modulus of elasticity E_g=640 kN/mm^2, Poisson's ratio v_g=0.21. There is no effect on the material properties due to temperature variations.

3. The effect of the radius of the glass on the maximum deformation is small.

4. The loading is a uniform pressure of w=0.10 N/mm^2 applied at the top of the panel. Gravity effects are ignored since the orientation of the panel is not known and the gravity load is small compared to atmospheric pressure.

5. The material properties used in the analysis are based on the assumption that the structure is built-in and deformed at room temperature and thermal expansion effects are ignored.

3.2. Triangular plate model

In order to prevent the physical contact of the plates, it is important to be able to predict the vertical deformation of the panel under atmospheric pressure for various values of the support spacing S and the plate thickness t. The triangular plate model is established to analyze the vertical elastic deformation of the thin plate panel between the consequent spacers.

In the triangular model, there are three symmetry axes (the angular bisectors). Fig. 1 shows one of the hexagons. The three symmetry lines are shown in one of the equilateral triangles. The crosshatched area indicates the portion of the plate that was modeled. The plate is discretized with 163 nodes and 143 four-node shell elements. This element has both bending and membrane capabilities. Each node has six degrees of freedom. The maximum element size is approximately the one forty spacing. The thickness t is constant. The total number of degrees of freedom is 978. All six degrees of freedom at the lower left node have been restrained. Also all nodes on the edge of the triangle have been restrained against translation in a direction, which is the normal to the edge direction. The slopes of all the nodes on the edges of the triangular plate along the edge direction and in direction normal to the panel are also restrained.

3.3. Beam model

In order to minimize the overall contact area of the panels, it is important to predict the contact
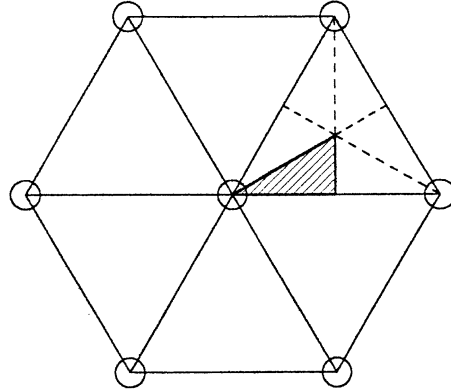
Fig. 1 Modeled portion of the panel

area under atmospheric pressure for various parameters: i.e., the spacing *S*, the radius of the spacer R_c and the thickness of the panel *t*. Although the triangular plate model is sufficiently good enough to predict the vertical deformations of the panel, it is not capable to evaluate the structural contact behavior between the thin plate and the spacers but the beam model is proper.

For the beam model, the deformation is axi-symmetric about a line normal to the plate passing through the center of the spacer. The plate is discretized with 908 nodes and 741 four-node elements. There are seven elements through the thickness of the panel close to the contact area and three elements through the thickness of the rest of the model. Fig. 2 shows the elements close to the
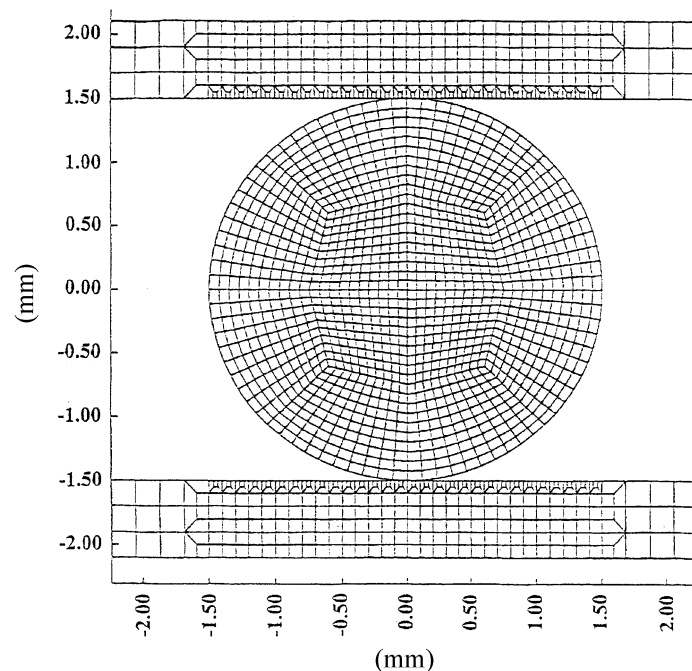

Fig. 2 Finite element model of a panel and spacer

sphere. Each node has two degrees of freedom. The total number of degrees of freedom is 1816. The material model was elastic-plastic with isotropic hardening (β=1) and with a constant tangent (or hardening) modulus E_t.

3.4. Rectangular plate model

Because the triangular plate and beam models are inadequate to estimate the stress distribution, the rectangular plate model is established to predict Von Misses stress distribution of the plate subjected to atmosphere pressure. Fig. 3 shows one of the hexagons of the panel in which four symmetric lines were selected in order to model a rectangular portion of the plate. The crosshatched area indicates the potion of the plate that is modeled. In this rectangular portion, there are five spacers, four in the corners and one at the center. It should be noted that the area of maximum deformation appears in white and has an almost triangular shape. If the area of maximum deformation is raised in advance (before deformation occurs), the maximum panel deformation will
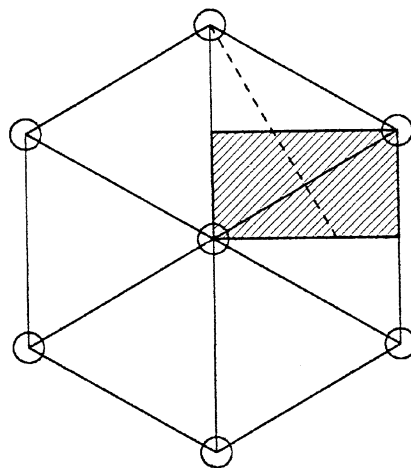

Fig. 3 Modeled portion of the panel
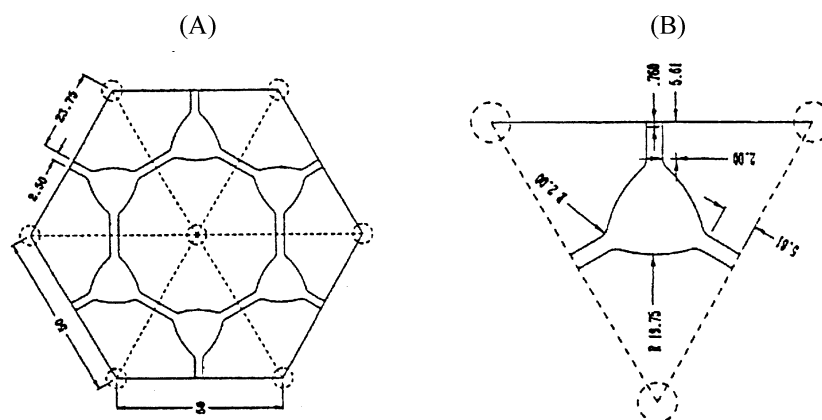
(A)   (B)

Fig. 4 Dimensions of an equilateral triangle of the rigidified geometry

be significantly reduced. Fig. 4(A) shows a top view of a hexagonal portion and 4(B) shows the dimensions of an equilateral triangle of the same geometry. The model contains 296 elements, 331
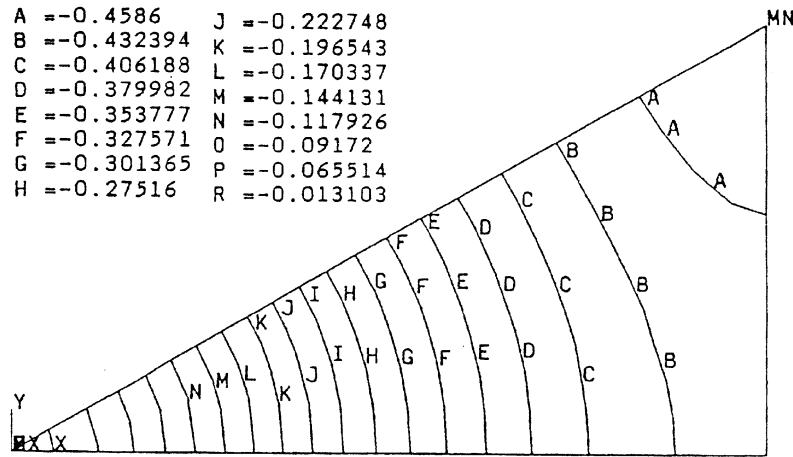


```
A =-0.4586       J =-0.222748
B =-0.432394     K =-0.196543
C =-0.406188     L =-0.170337
D =-0.379982     M =-0.144131
E =-0.353777     N =-0.117926
F =-0.327571     O =-0.09172
G =-0.301365     P =-0.065514
H =-0.27516      R =-0.013103
```

Fig. 5 Vertical deformation distribution of the panel for S=50 mm and t=0.6 mm

Table 1 Maximum panel sag (mm) for different E_s

S		t
		0.2	0.4	0.5	0.6	0.8	1.0
10	E_{s1}	0.0252	0.0032	0.0016	0.0009	0.0004	0.0002
	E_{s2}	0.0239	0.0030	0.0015	0.0009	0.0004	0.0002
20	E_{s1}	0.2502	0.0504	0.0259	0.0150	0.0063	0.0032
	E_{s2}	0.2430	0.0479	0.0246	0.0143	0.0060	0.0031
30	E_{s1}	0.5588	0.2273	0.1280	0.0755	0.0321	0.0164
	E_{s2}	0.5466	0.2182	0.1220	0.0718	0.0305	0.0156
40	E_{s1}	0.8957	0.5040	0.3482	0.2272	0.1007	0.0518
	E_{s2}	0.8780	0.4896	0.3352	0.2180	0.0960	0.0493
50	E_{s1}	1.2612	0.8037	0.6301	0.4712	0.2389	0.1259
	E_{s2}	1.2374	0.7845	0.6120	0.4544	0.2280	0.1197
60	E_{s1}	1.6507	1.1175	0.9283	0.7561	0.4546	0.2560
	E_{s2}	1.6204	1.0933	0.9056	0.7344	0.4364	0.2439
70	E_{s1}	2.0606	1.4469	1.2377	1.0534	0.7209	0.4502
	E_{s2}	2.0235	1.4172	1.2099	1.0271	0.6968	0.4309
80	E_{s1}	2.4883	1.7915	1.5592	1.3599	1.0081	0.6964
	E_{s2}	2.4440	1.7560	1.5261	1.3345	0.9792	0.6704
100	E_{s1}	3.3910	2.5223	2.2393	2.0030	1.6037	1.2601
	E_{s2}	3.2210	2.4795	2.1949	1.9612	1.5689	1.2241
120	E_{s1}	4.3711	3.3014	2.9651	2.6872	2.2351	1.8566
	E_{s2}	4.2949	3.2407	2.9086	2.6339	2.1865	1.8111

E_{s1}: E_s=200000 N/mm², v=0.3, p=0.1 N/mm²
E_{s2}: E_s=195000 N/mm², v=0.3, p=0.1 N/mm²

nodes and 1986 degrees of freedom.

4. Numerical results

Based on the finite element models and programs, the deformational characteristics of the panel such as the vertical deformation of the plate between spacers, the contact area of the plate and the spacer, as well as the stress distribution are found.

4.1. Vertical deformation

To estimate the vertical deformation between consequent spacers, the triangular plate model and the Newton-Raphson algorithm are implemented with displacement convergence criterion of 0.001 mm. The maximum sag z was found for t=0.2, 0.4, 0.5, 0.6, 0.8, and 1.00 mm and for S=10, 20, 30, 40, 50, 60, 70, 80, 100, and 120 mm. The contour plot of vertical deformation of the panel for S=50 mm and t=0.6 mm is shown in Fig. 5. The numerical results indicate that the maximum deformation occurs around the midpoint of the panel between two spacers. The vertical deformation is gradually decreased near the spacer. The deformation of the location away from the spacer is nonlinear. Table 1 presents the maximum deformation (sag) z for various values of the thickness t and spacing S.
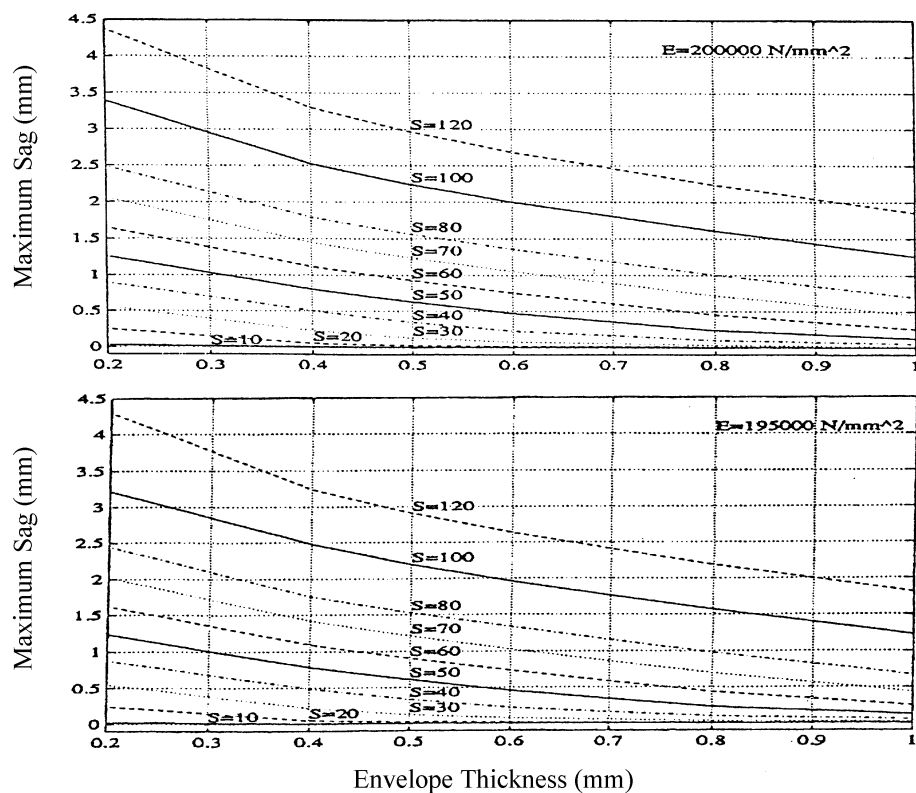

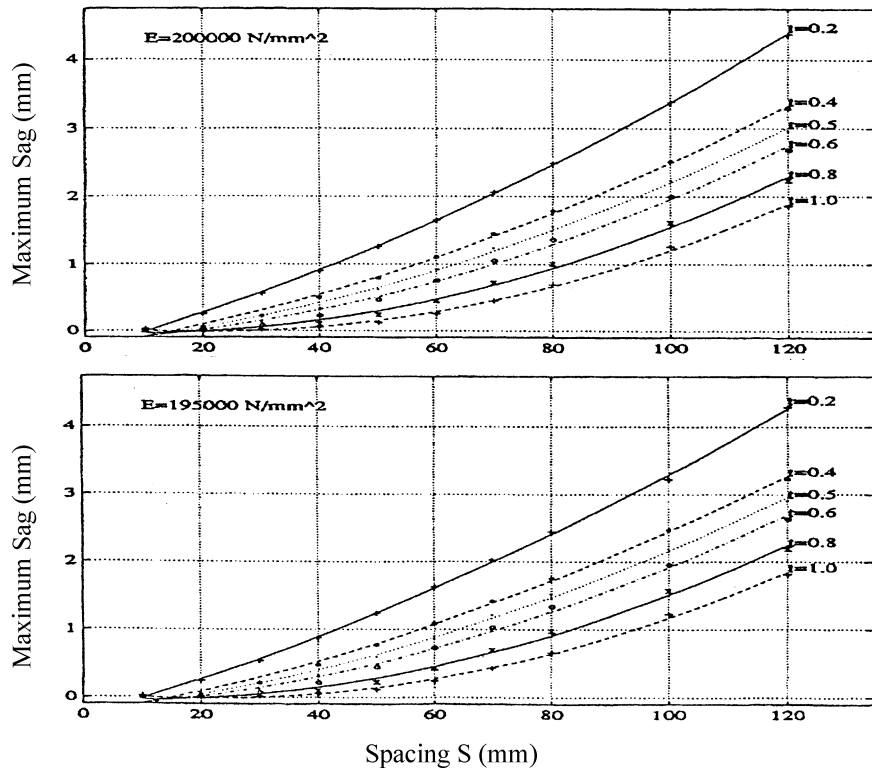Fig. 6 Sag z versus thickness t for various valuse of S

Fig. 7 Maximum sag *z* versus spacing *S* for various values of *t*

Fig. 6 gives the maximum sag versus the thickness *t* for various values of the spacing *S* and Fig. 7 gives the maximum sag versus the spacing *S* for various values of the thickness *t*. The data points were generated by using the nonlinear elastic finite element analysis and the continuous lines are second order polynomials that fit the generated data in a least squares sense. The materials having different modulus of elasticity have the same profile of the maximum sag versus spacing curve. The figures indicate that the maximum deflection increases as the thickness of the plate decreases. Fig. 8 presents a set of interaction curves used to evaluate the maximum sag for any pair on *S* and *t*. The interaction curves are spaced every 0.15 mm of deflection *z* apart. In conclusion, the maximum sag for any practical range of values *S* and *t* can be predicted by using the above mentioned figures.

4.2. Contact area

To find the contact area, the beam model and the Broyden-Fletcher-Goldfarb-Shanno (BFGS) Formulation and Algorithm for nonlinear problem solution method were implemented with convergence tolerance on displacements of 0.001 mm. A comparison of the contact radius results obtained by the above-described model and the available experimental data is shown in Table 2. The parameters such as thickness, diameter, spacing, modulus of elasticity, and yield stress are also included in Table 3. Fig. 9 shows the contact radius R_c versus spacing *S* for the experimental data, the finite element results, hardness estimate, and the Hertz formulation. The error between the experimental data and the finite element solution varies between 2 % and 17%.
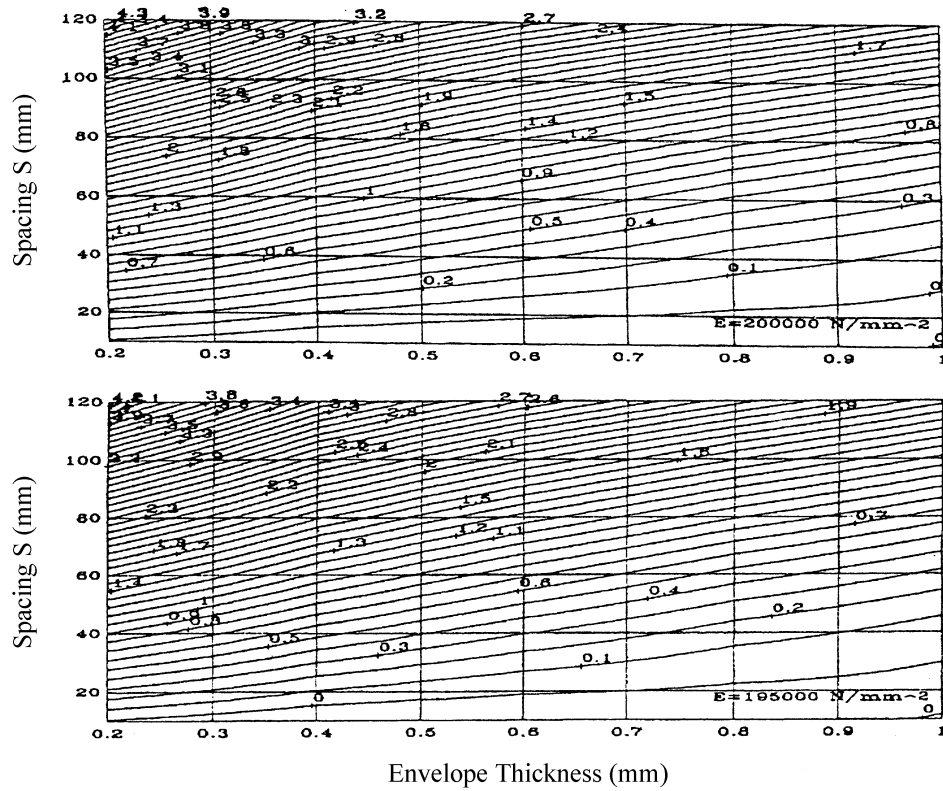
Fig. 8 Interaction curves *S-t* for determining sag *z* (mm) with different E_s

Table 2 Contact radius-comparison Hertz, Hardness, and FEA results

Material	Measured Lab. R_{cont} (mm)	Model			
		Hardness R_{cont} (mm)	Hertz R_{cont} (mm)	FEA	
				R_{cont} (mm)	Z_{sag} (mm)
6061Al	0.280±.030	0.425	0.268	0.26	0.027
Copper	0.350±.070	0.266	0.185	0.24	0.021
304SS	0.333±.019	0.430	0.232	0.34	0.049
SN-CRS	0.154±.016	0.105	0.088	0.142	0.015
SN-CRS	0.307±.021	0.215	0.142	0.251	0.17
SN-CRS	0.550±.000	0.292	0.175	0.452	0.64
SN-CRS	0.690±.019	0.433	0.232	0.675	1.20

It is apparent that the effect of the diameter *D* on the maximum sag *z* is negligibly small. The parameter that mainly influences the maximum sag is the spacing *S*. The effect of the tangent or hardening modulus E_t on the contact radius R_c for *S*=80 mm, *t*=0.6 mm, and σ_y=276 N/mm^2 has been found. For this case and with values of E_t=1.0 N/mm^2, 200.0 N/mm^2, 600.0 N/mm^2 and 2000.0 N/mm^2, the corresponding values of R_c are 0.675 mm, 0.6125 mm, 0.572 mm, 0.360 mm, respectively.

Table 3 Contact radius-comparison of experimental, and Hertz, Results

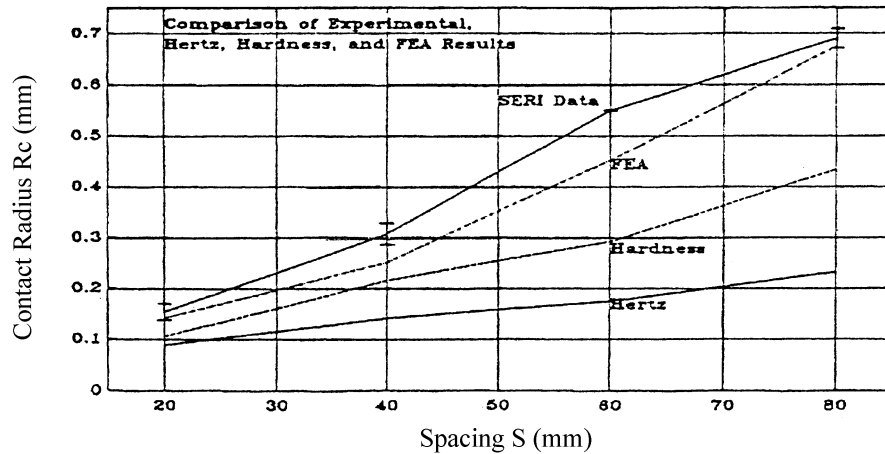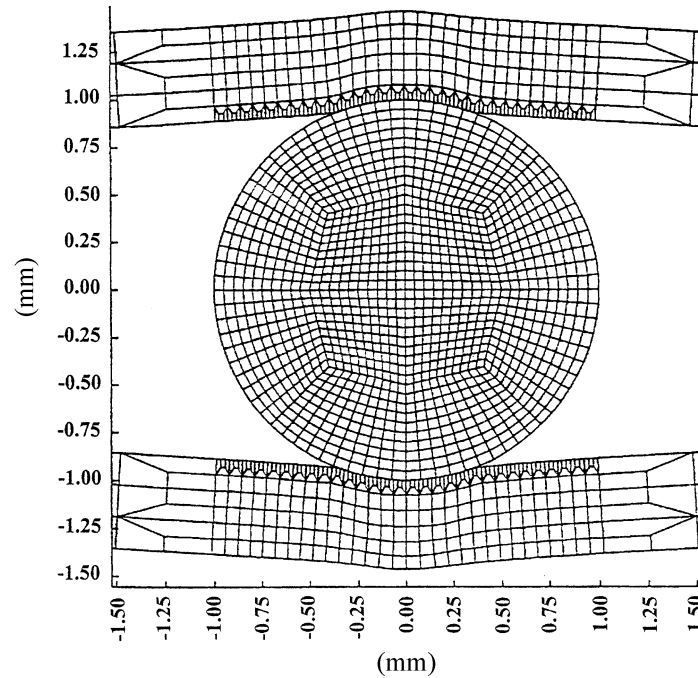| Material	t (mm)	D (mm)	S (mm)	Young's Modulus E (N/mm^2)	Brinell Hardness BH	Yield Stress σ_y (N/mm^2)
6061Al	3	3	50	69000	113	346
Copper	3	3	50	115000	111	340
304SS	3	3	80	190000	161	494
SN-CRS	0.6	3	20	200000	92	276
SN-CRS	0.6	3	40	200000	92	276
SN-CRS	0.6	3	60	200000	92	276
SN-CRS	0.6	3	80	200000	92	276

Fig. 9 Contact radius versus spacing for experimental FEA, Hertz and Hardness results

The contact radius R_c and the maximum sag z were found for t=0.2, 0.4, 0.5, 0.6, 0.8, and 1.00 mm and for sphere diameters D=2, 4, 6, 8, and 10 mm. Fig. 10 shows the deformed shape of the beam model. The deformed-shape, undeformed-shape, and the thinning of the panel can be observed. The parameters are presented in Table 4 such as the contact radius R_c for spacing S=40, 50, 60 and 80 mm, the various values of the spacer diameter D=2, 4, 6, 8 and 10 mm, and the envelope thickness t.

Fig. 11 shows the contact radius R_c versus the envelope thickness t for S=40, 50, 60 and 80 mm, and various values of the spacer diameter D. As expected the contact radius reduces as the thickness increases. Any further increase in the thickness does not reduce the contact radius, if S=40 mm after a critical thickness of about 0.5 mm, if S=50 mm after a critical thickness of about 0.7 mm, or if S =60 mm after a critical thickness of about 0.9 mm. For S=80 mm, there is no noticeable critical thickness. As the spacer diameter increases, the contact radius increases. For smaller values of t, the increment is significant. The results have also been curve fit to predict the contact radius R_c for a given set of D and t. The fifth order spline which gives the minimum potential energy is also derived. Table 5 shows the contact radius polynomials for S and D. In all above parameter

Fig. 10 Deformed shapes of the panel and the spacer at p=0.1 N/mm^2

Table 4 Contact radius R_c (mm) nonlinear elastic-plastic analysis

D (mm)	S (mm)	Envelope thickness t (mm)					
		0.2	0.4	0.5	0.6	0.8	1.0
2	40	0.4600	0.2500	0.2400	0.2370	0.2300	0.2200
	50	0.5900	0.3900	0.3260	0.2900	0.2500	0.2500
	60	0.7300	0.5337	0.4555	0.3900	0.2961	0.2500
	80	1.1000	0.7000	0.6200	0.5700	0.4900	0.4400
4	40	0.6100	0.3300	0.3000	0.2850	0.2710	0.2700
	50	0.7900	0.4700	0.3923	0.3403	0.3200	0.3100
	60	0.9600	0.6100	0.5247	0.4390	0.3408	0.3000
	80	1.3200	0.9100	0.7500	0.6500	0.5500	0.4800
6	40	0.7200	0.3600	0.3200	0.3000	0.2910	0.2900
	50	0.9300	0.5601	0.4500	0.3800	0.3550	0.3500
	60	1.1500	0.7433	0.6084	0.5100	0.3855	0.3500
	80	1.5500	1.0500	0.8660	0.7300	0.5900	0.5400
8	40	0.7500	0.3900	0.3400	0.3300	0.3300	0.3300
	50	1.0396	0.6300	0.5000	0.4050	0.3700	0.3700
	60	1.2800	0.8783	0.7018	0.6200	0.4322	0.4000
	80	1.8200	1.2300	0.9700	0.7846	0.6600	0.6200
10	40	0.8000	0.4300	0.4130	0.4120	0.4100	0.4100
	50	1.2000	0.7800	0.6132	0.4984	0.4300	0.4300
	60	1.5400	0.9655	0.7800	0.6413	0.4789	0.4500
	80	1.9000	1.2400	0.9900	0.8193	0.6800	0.6400

Steel: E_s=195000 N/mm^2, v_s=0.3, σ_y=300 N/mm^2, E_t=1000 N/mm^2, β=1, T=70°F

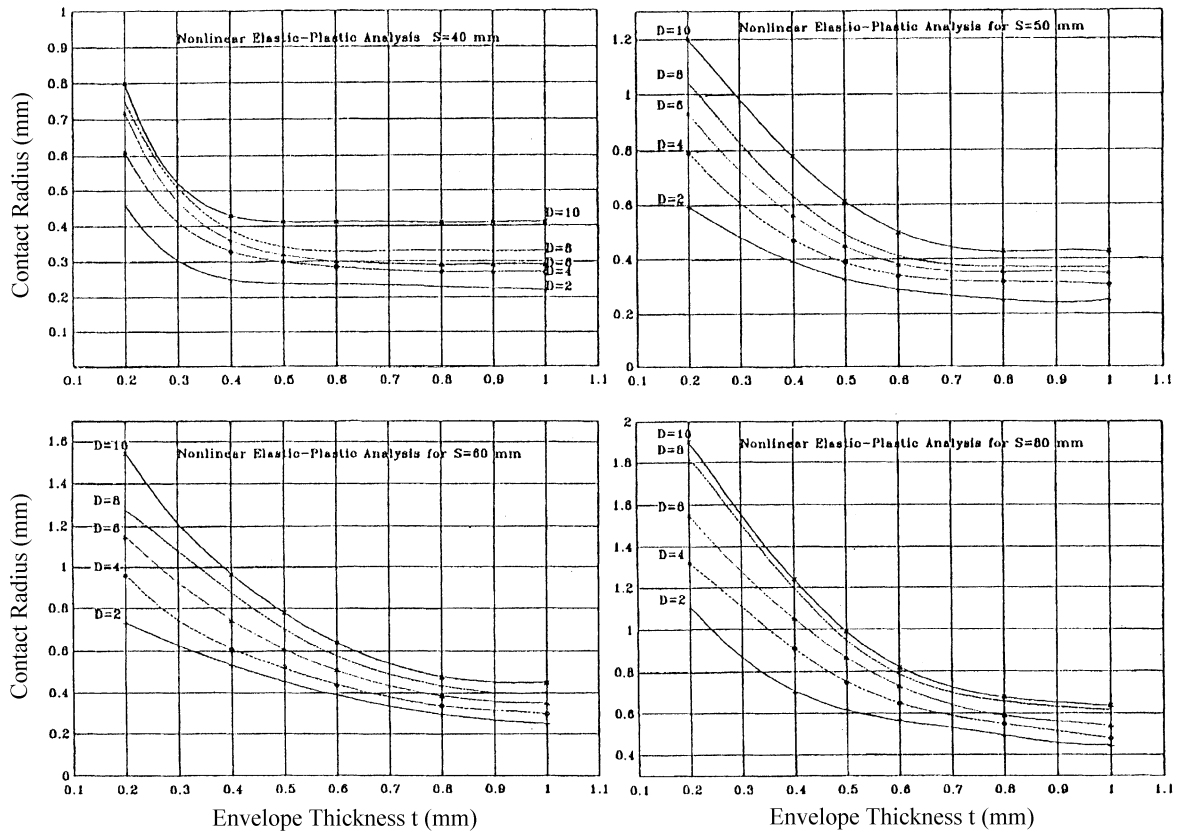Glass: E_g=64000 N/mm^2, v_g=0.21, T=70°F, p=0.1 N/mm^2

Fig. 11 Contact radius versus thickness for various *S*

combinations (120 total), the maximum panel displacement (sag z) is found. Fig. 12 shows the maximum sag *z* versus the envelope thickness *t* for all the values of *S* and *D*.

4.3. Rigidity of the panel

To investigate the stress distribution, the interaction between the deformation and the stress distribution is one of the most important factors for the materials nonlinearity. A rectangular finite element model of this geometry has been established and analyzed. The parameters used are: S=50 mm, t=0.66 mm. Based on the modified rectangular plate model, the maximum sag was found for various values of the rise h (h=0.0, 0.2, 0,4, 0.6, 0.8 and 1.0 mm). The effect of the rise h on the maximum sag of the rigidity of the structure is shown on Table 6. For small rise (h=0.2 mm) a 50% reduction of the maximum sag of the flat panel is observed. Any further increase in the rise does not produce any significant reduction of the maximum sag.

4.4. Optimum supported patterns

To minimize the overall contact areas, it is not only to reduce the contact area between the plates and the spacers but also to reduce the number of the spacers. Based on the minimum stress
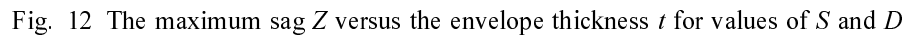
Table 5 Contact radius polynomial

D (mm)	S (mm)	$R_c(t)=c_1t^5+c_2t^4+c_3t^3+c_4t^2+c_5t+c_6$
2	40	$R_c = -10.9375t^5+37.5521t^4-50.6458t^3+33.5604t^2-10.9692t+1.6600$
	50	$R_c = 6.3205t^5-18.4898t^4+19.7166t^3-8.45880t^2+0.45840t+0.7074$
	60	$R_c = -0.32490t^5+0.80570t^4-0.74950t^3+0.97320t^2-1.4383t+0.9847$
	80	$R_c = 8.25830t^5-21.4392t^4+17.6529t^3-2.49730t^2-3.2830t+1.7563$
4	40	$R_c = -10.5903t^5+36.6146t^4-49.9444t^3+33.8813t^2-11.6128t+1.9217$
	50	$R_c = 2.1946t^5-6.81504t^4+6.19430t^3+0.17500t^2-2.73370t+1.2941$
	60	$R_c = -10.2262t^5+33.5346t^4-42.8822t^3+27.5737t^2-9.8222t+2.1202$
	80	$R_c = 8.52510t^5-29.0784t^4+36.1306t^3-18.5303t^2+2.0256t+1.4070$
6	40	$R_c = -15.7986t^5+52.7604t^4-69.6319t^3+45.9229t^2-15.4044t+2.4417$
	50	$R_c = 3.3994t^5-12.1961t^4+14.6213t^3-5.39600t^2-1.41070t+1.3301$
	60	$R_c = 0.888800t^5-2.08060t^4+0.72230t^3+2.71370t^2-3.6668t+1.7755$
	80	$R_c = -1.4507t^5+2.30950t^4-0.97440t^3+2.17890t^2-3.7382t+2.2136$
8	40	$R_c = 3.819400t^5-6.77080t^4-1.38890t^3+9.43750t^2-6.45060t+1.6833$
	50	$R_c = 8.8847t^5-29.8915t^4+36.4141t^3-17.8182t^2+1.59033t+1.1911$
	60	$R_c = 8.862200t^5-29.4411t^4+37.0595t^3-20.1514t^2+2.8065t+1.2688$
	80	$R_c = 14.1691t^5-49.1249t^4+62.7772t^3-33.7429t^2+4.7494t+1.7901$
10	40	$R_c = -16.5625t^5+58.0729t^4-80.0833t^3+54.3521t^2-18.1852t+2.8160$
	50	$R_c = 2.1130t^5-11.1634t^4+18.0443t^3-10.2251t^2+0.22370t+1.4337$
	60	$R_c = -2.31890t^5+7.96500t^4-11.5407t^3+10.6653t^2-6.8962t+2.5781$
	80	$R_c = 8.31920t^5-30.0550t^4+39.0873t^3-19.8111t^2+0.8428t+2.2539$

Steel: E_s=195000 N/mm^2, v_s=0.3, σ_y=300 N/mm^2, E_t=1000 N/mm^2, β=1, T=70°F

Glass: E_g=64000 N/mm^2, v_g=0.21, T=70°F, p=0.1 N/mm^2

distribution and vertical deformation, the optimum supported pattern has been found to reduce the overall contact area of the panel.

In order to investigate the effect of the optimum supported conditions, two whole panels are modeled, one with a square pattern of spacers and one with a hexagonal pattern. The vertical deformational distribution of the square pattern panel is shown in Fig. 13(A). From this figure one can observe that for all interior spacers there is a symmetric deformation and also a channel of large deformation is formed along the perimeter. This can be prevented if a cantilever portion of the panel was designed to balance the pressure load in either side of the first (and last) row (and column) of the spacers. The optimum length of the cantilever portion can be found easily if the geometry of the panel in known.

Fig. 14 shows the dimensions of a rectangular (457.2 mm × 398.25 mm) panel with a hexagonal pattern of spacers. Fig. 13(B) shows the vertical deformation of the original design (without spacers A and B) in which maximum deformation is 39.4 mm. Fig. 13(C) shows the vertical deformation of the modified design (without spacer A) in which the maximum deformation is 35.2 mm. Fig. 13(D) shows the vertical deformation of the final design shown in Fig. 14 (with all the spacers) in which maximum deformation is 4.4 mm. In conclusion, an optimum supported pattern and an optimum cantilever length based on the number of spacers reduce the stress distribution and vertical deformation in order to avoid large deformation and consequently plate contact.

Fig. 12 The maximum sag Z versus the envelope thickness t for values of S and D

Table 6 Effect of rise h on the maximum sag of the rigidified structure

h (mm)	Linear				Non-linear	
	Thin shell		Thick shell		Thin shell	
	z_{max}	$\sigma_{e,max}$	z_{max}	$\sigma_{e,max}$	z_{max}	$\sigma_{e,max}$
0.0	0.762	1819	0.79132	1359	0.6284	1229
0.2	0.4319	1464	0.437403	1057	0.3657	1301
0.4	0.4146	1408	0.420302	1049	0.3490	1298
0.6	0.4010	1404	0.406947	1045	0.3400	1300
0.8	0.3921	1402	0.398109	1043	0.3362	1300
1.0	0.3866	1402	0.392456	1043	0.3362	1303

S=50 mm, t=0.66 mm, E=200000 N/mm^2, v=0.3

5. Recommendations to be a 'smart' structure

This designed panel saves space, energy, and displaces harmful chlorofluorocarbons. It is more fascinating if the concept of controlled insulation is feasible. In other words, a panel which will act as an insulator only for a given range of temperatures, and as a conductive plate for the rest of the temperatures is useful. In an effort to demonstrate the feasibility of an automatically variable structural panel, a finite element model of a simple panel consisting of two plates is established. Each plate is composed of two layers of materials with different coefficients of thermal expansion α^{top}=92 × 10^{-7}°C^{-1} and α^{bot}=70 × 10^{-7}°C^{-1}. Fig. 15(A) shows the finite element model. Three loading
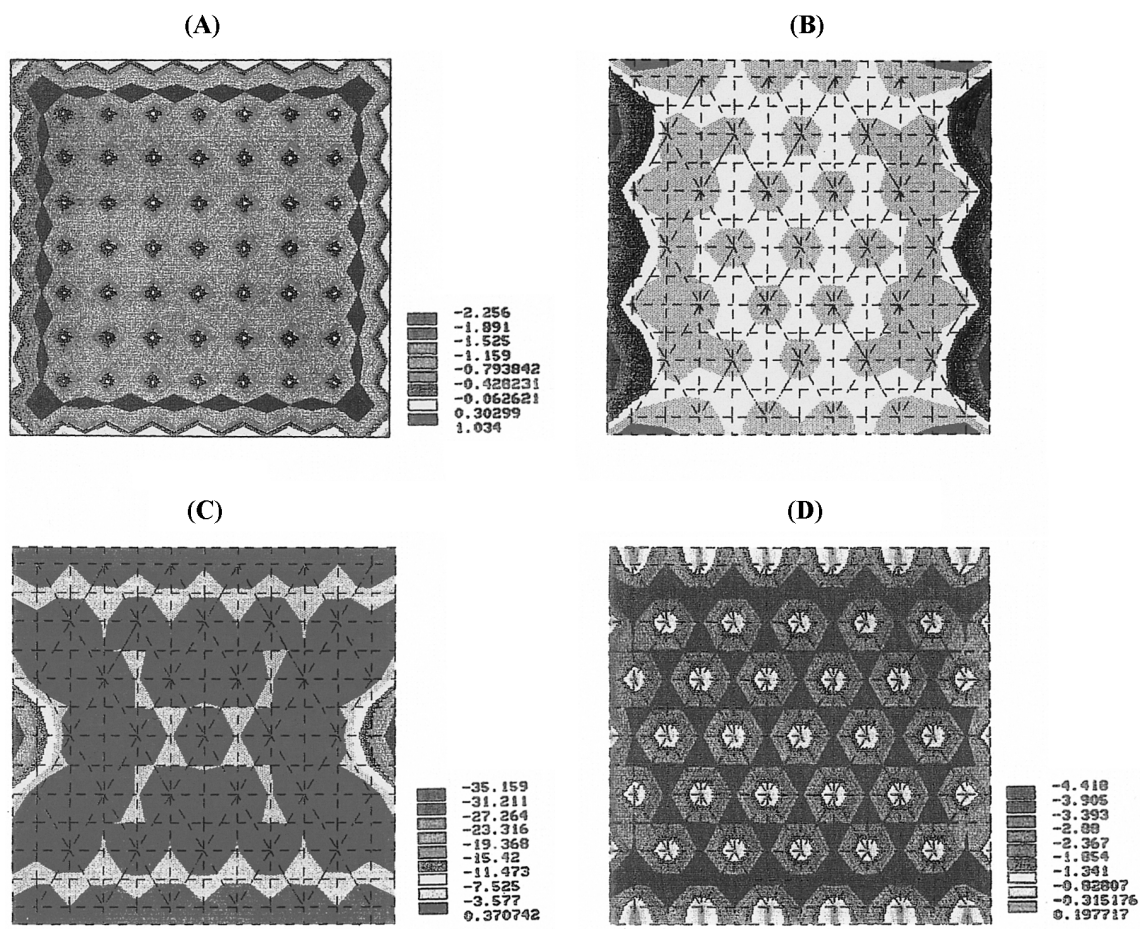
(A)

(B)

(C)

(D)

Fig. 13 Vertical deformation of the whole panel with square pattern
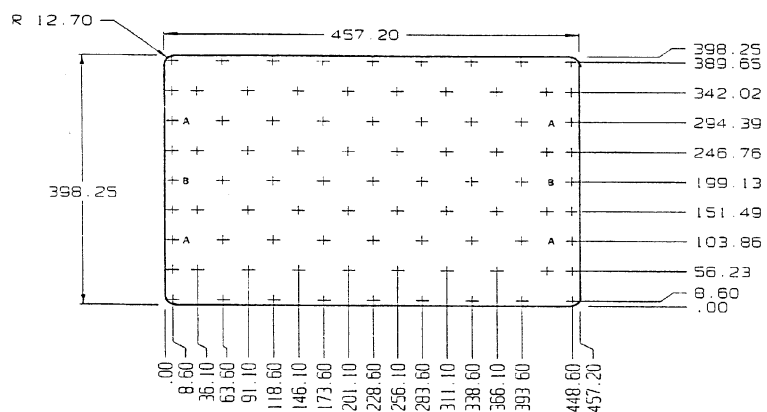
Fig. 14 Dimensions of the whole panel with hexagonal pattern

conditions are considered. First, at a reference temperature of 70°C, a uniform pressure of 0.1 N/mm^2 is applied. The deformed shape is shown in Fig. 15(B). Second, the pressure and an outside
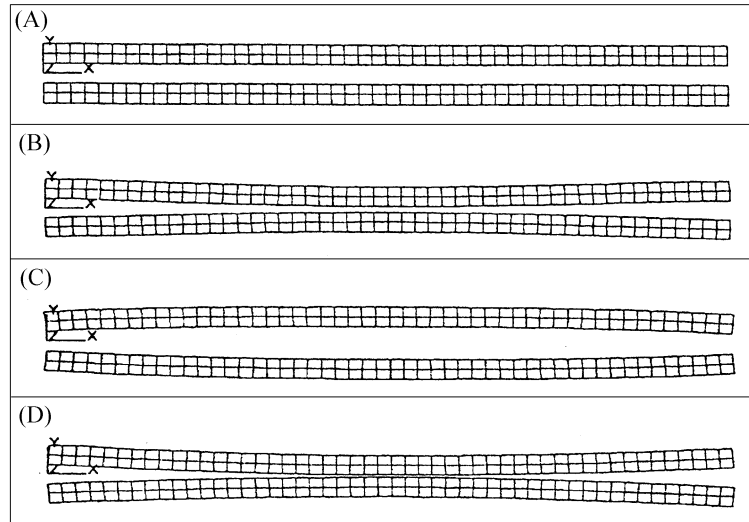
Fig. 15 Vertical deformation of the thermo-structural model

temperature of 350°C was applied. The deformed shape is shown in Fig. 15(C). Finally, the pressure and an outside temperature of 350°C were applied. The deformed shape is shown in Fig. 15(D).

Fig. 15 indicates that if the structure serves as an isolator for high temperature variation, the thermal effects are significant. The temperature variation may create the interaction of these nonlinearities. In the further research, the composite material with low coefficient of thermal expansion may reduce the thermal effects of this type of panel. Moreover, the characteristics of thermal effects may enhance the stiffness of the panel to resist the atmosphere pressure if the temperature is much greater than room temperature. On the other hand, the thermal effects may reduce the stiffness of the panel to resist the atmosphere pressure if the temperature is much less than room temperature depending on the design.

6. Conclusions

Based on the previous work, the most important conclusions are as follows:

For modeling: The four finite element models provided in this paper indicate the philosophy of a finite element modeling and predict the trend of structural behavior. A proper virtue simulation reduces the laboratory costs − especially for a complicated structure like this panel. Based on the structural characteristics, the finite element models established in this paper are capable to estimate the structural behavior.

For mainly parameter of vertical deformation: The effect of the diameter D is negligibly small for the maximum vertical deformation of the plate panel. The parameter that mainly influences the maximum sag is the spacing between the spacers. The maximum vertical deformation of the panel can be predicted for a practical range of parameters S and t by the figures provided in this paper.

For the thickness of plate: As the thickness of the plate is increased, the vertical deformation between the two sequent spacers decreases and the contact radius also decreases. As the plate reaches the critical thickness, any further increment does not produce any significant contact radius

of the panel.

For the pre-rise of the plate: The stress distribution and the vertical deformation are always interacted. Based on the modified rectangular plate model, the maximum sag is significantly reduced by pre-rise of h. If the rise of h reaches its critical high, any further increment does not produce significant reduction of the maximum sag.

For the optimum supported patterns: The optimum supported patterns reduce the stress distribution and vertical deformation based on the number of spacers and the optimum cantilever length. The optimum supported patterns are to avoid large deformation and consequently plate contact. For this type of panel, it is essential to establish the optimum support patterns.

For smart structure: The design of a smart structure is possible by using bimetallic and careful design considering the thermal and structural effects simultaneously. If the panel serves as an isolator for high temperature variation, composite materials with low coefficient of thermal expansion reduce the thermal effects. The thermal effects may enhance the stiffness of the panel in a proper design.

As the environmental protection attracts a lot of attentions, it is important to save energy by isolating temperature conductance in many applications. It is the way to study the panel like this to contribute the energy saving.

References

Bathe, K.-J. (1982), *Finite Element Procedures in Engineering Analysis*, Prentice-Hill, Inc.

Hua, C.-H. and Wang, Y.-C. (1997), "Element type effects on stability analysis of plates", *Proceedings of 1997 ANSYS User Conference*, Nov. 4-5, Taiwan, No. 4, 1-10.

Shu, H.-S., Wang, Y.-C. and Wei, C. (1997), "Modelling of thin plates under uniform pressure with boundary nonlinear condition", *Proceedings of the Fourth Military Academy Symposium on Fudamental Science*, Taiwan, 1175-1184.

Ugural, A.C. (1981), *Stresses in Plates and Shells*, McGraw-Hill Book Company.

Vlahinos, A.S., Ermopoulos, J.C.H. and Wang, Y.-C. (1991), "Buckling analysis of trapezoidal thin plates", *Proceedings of 1st National Conference on Steel Structures*, Athens, Greece, June 6-7, 98-110.

Wang, Y.-C. and Vlahinos, A.S. (1995), "Response of thin plates under pressure and hexagonal support pattern", *Proceedings of the Eighth Pacific Conference on NDT*, Taiwan December, 695-702.

Wei, C. and Wang, Y.-C. (1995), "Modelling of compact vacuum insulators", *Chinese Military Academy Journal*, **30**(2), 261-270.